Flying Capacitor Design Considerations for a 48-to-12 V, 35 A Split-phase Dickson SC Converter

Richard(*Yue*) *Sun*[*], *Samuel Webb and Yan-Fei Liu*
(Department of Electrical and Computer Engineering, Queen's University, Kingston K7L 3N6, Canada)

Abstract: Switched-capacitor converters can deliver better performance, power density, and switch utilization compared to inductor-based power converters, but they suffer from current spikes during switching due to capacitor charge redistribution. This can be solved by methods such as split-phase control, which was developed to address charge redistribution in Dickson SC converters by controlling the charging and discharging of the circuit's flying capacitors, such that the equivalent branch voltages line up when the circuit switches states. However, split-phase control is most effective at compensating for charge redistribution when all the circuit's flying capacitors are matched in capacitance value. Differences between the capacitance values of the circuit flying capacitors may result in split-phase control not being able to fully compensate for charge redistribution, due to the different charge/discharge rates of the flying capacitors. The work presented in this paper provides an in-depth analysis of the sensitivity of the split-phase Dickson converter to mismatches in flying capacitor values, as well as discussions regarding the design considerations and prototype test results of a split-phase Dickson converter for high-current loads.

Keywords: Switched-capacitor converter, Dickson converter, split-phase control, capacitor mismatch

1 Introduction

The emerging 48-volt power architecture for data centers has the potential to offer up to 30% reduction in conversion losses, as well as up to 16 times reduction in distribution losses throughout the server rack [1]. However, for these reductions to be fully realized, better voltage conversion technology is required to bridge the gap between the new 48-volt infrastructure and the existing 12-volt infrastructure. Traditional inductor-based step-down power converter topologies are bulky, with power densities generally between 50 W/in^3 and 200 W/in^3 [2-3]. For this reason, inductor-less DC-DC converter topologies, such as the switched-capacitor converter, has seen a resurgence of interest from researchers as they offer better space utilization [4-5], through reduced reliance on magnetic components [6], reduced component stress [7-8], as well as better switch utilization [9] and simple control [10]. However, switched-capacitor converters are particularly vulnerable to problems relating to capacitor charge redistribution [6], where the closing of a switch between capacitors with unequal voltages result in significant current spikes [11-12]. Charge redistribution not only contributes to power losses [13-16], but in higher-power applications, may lead to component breakdown as well. Such applications would therefore require large flying capacitor values and/or high switching frequencies to mitigate charge redistribution. However, utilizing large flying capacitors reduces the power density of the switched-capacitor converter, and utilizing high switching frequencies results in increased switching losses and potential electromagnetic interference [17]. The problem of charge redistribution has thus far precluded the use of switched-capacitor converters outside of low-power applications [10].

The split-phase control theory [18] was developed to overcome the charge redistribution problem in the Dickson switched capacitor converter (Fig. 1) without needing to implement

Manuscript received September 18, 2020; revised November 14, 2020; accepted November 19, 2020. Date of publication December 31, 2020; date of current version November 30, 2020.
* Corresponding Author, E-mail: sun.richard@queensu.ca
Digital Object Identifier: 10.23919/CJEE.2020.000028

large capacitors or high switching frequencies. In traditional two-phase operation (where all switches have 50% duty cycles), the branch voltages of the equivalent circuits exhibit large differences before switching takes place, resulting in significant current spikes as a result. Split-phase control eliminates the branch voltage differences by setting slightly lower duty cycles on some of the circuit's switches. This allows the charging and discharging of the flying capacitors to be controlled, such that the branch voltages are equalized before switching takes place. Both the conventional two-phase [19-20] and the split-phase [14-15,18] have seen implementations, however these have generally been either for low-current applications of no more than 10 A [14-15,18,20] or utilize large flying capacitors to mitigate the effects of charge redistribution [19].

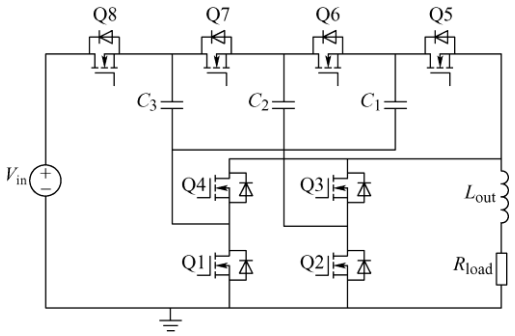

Fig. 1 4-to-1 step-down Dickson SC converter schematic

In adapting the split-phase Dickson SC converter for a 48 V to 12 V step-down, 35 A application, it has been determined that the split-phase Dickson SC converter is very sensitive to mismatches in the circuit's flying capacitors. As mentioned previously, split-phase control relies on the control of the charging and discharging of the flying capacitors to eliminate charge redistribution. If the flying capacitors are mismatched in capacitance, the branch voltages at the time of switching will not be equal. Without the addition of significant control complexity, the uneven charging and discharging can in turn result in branch voltage differences during switching. Flying capacitor mismatch can therefore result in split-phase control not fully compensating for charge redistribution. It is thus imperative that the flying capacitors be designed such that they are matched in capacitance as closely as possible.

Regarding the design of split-phase Dickson converters, typically, ceramic capacitors are used to construct the flying capacitors for SCCs because of their low ESR values and high capacitance-to-volume ratio. However, ceramic capacitors are known to lose capacitance when subjected to a DC bias voltage. This property, in addition to typical manufacturing tolerances of ±20%, makes exactly matching the flying capacitors, each of which will have a different DC blocking voltage in the Dickson SCC, difficult in practice.

Prototype testing has shown that, while the split-phase Dickson converter was able to operate reliably with up to 30% variances in capacitance between the flying capacitors, operation with fully-matched flying capacitors resulted in an increase in efficiency and a decrease in the maximum observed temperature at full load operation. The prototype with matched flying capacitors achieved a full load efficiency of 96.3% at 48 V to 12 V, 35 A operating conditions.

The remainder of this paper is structured as follows. Section 2 provides a brief overview of the operation of the 4-to-1 Dickson converter, Section 3 provides simulation analysis of the impact of flying capacitor size mismatch on the operation of the split-phase Dickson converter, Section 4 discusses practical design considerations for the split-phase Dickson converter, as well as a derivation of an in-circuit flying capacitance estimation method based on voltage waveforms obtained in testing. Finally, Section 5 discusses the test results of a 4-to-1 split-phase Dickson converter prototype.

2 Overview of topology and split-phase control

In traditional two-phase operation of the Dickson converter, all switches have a duty cycle of 0.5. For a 4-to-1 Dickson SC converter (Fig. 1), during the first half of the switching cycle (henceforth referred to as Phase 1), switches Q8, Q6, Q4, and Q2 are turned on, while the remaining switches are off. During the second half of the switching cycle (Phase 2), switches Q7, Q5, Q3, and Q1 are turned on, while the remaining switches are off. Two-phase operation results in two equivalent circuits, as shown in Fig. 2 [18].

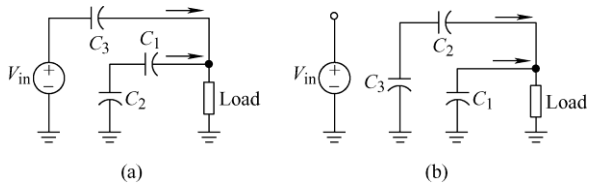

Fig. 2 Two-phase equivalent circuits of 4-to-1 Dickson converter

As previously discussed, two-phase operation of the Dickson converter can result in large current spikes during switching due to charge redistribution. Simulations of two-phase operation of the 4-to-1 Dickson SC converter has shown that there are significant differences between the equivalent circuit branch voltages during switching. The branch voltages of the equivalent circuit for Phase 1 (Fig. 2a), (V_{in}–V_{C3}) and (V_{C2}–V_{C1}), are divergent before the circuit transitions to Phase 1, Charge redistribution occurs as the branch voltages quickly equalize after switching takes place, as shown in Fig. 3. The behavior of the branch voltages for Phase 2, (V_{C3}–V_{C2}) and V_{C1}, are similarly affected. The current spikes resulting from charge redistribution not only contribute to power losses, but in high power applications may cause damage to circuit components. Simulation parameters used are shown in Tab. 1.

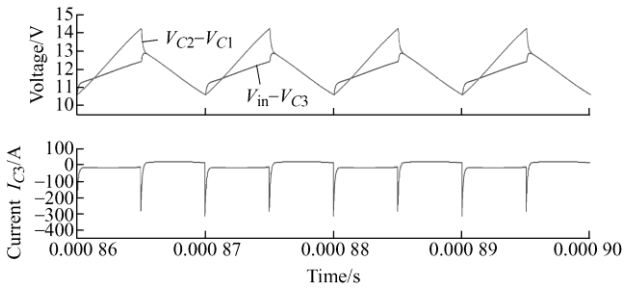

Fig. 3 Simulated Phase 1 branch voltage and flying capacitor C_3 behavior of two-phase 4-to-1 Dickson converter

Tab. 1 Simulation parameters

Parameter	Value
Input voltage V_{in}/V	48
Output current I_{out}/A	35
Flying capacitor nominal sizes C_3, C_2, C_1/μF	47
Output capacitor size C_{out}/μF	47
Output inductor size L_{out}/nH	200
Switching frequency f_{sw}/kHz	100
MOSFET on-resistance $R_{DS(on)}$/mΩ	1
Flying capacitor equivalent series resistance R_{ESR}/mΩ	1
Output inductor winding resistance $R_{L(winding)}$/mΩ	0.3

In split-phase control [18], reduced duty cycles are used on some of the circuit's switches, such that these switches are switched off earlier than other switches they are in phase with. This therefore introduces additional circuit states in which a single flying capacitor branch's charging and discharging is directly controlled. The duty cycle to be imposed on the 'split-phase' switches are dependent on the circuit's conversion ratio. As seen in the derivations shown in Ref. [18], the duty cycle to be implemented on the 'split-phase' switches for a Dickson converter with an N-to-1 conversion ratio and matched flying capacitor values can be calculated using Eq. (1).

$$D_{\text{split-phase}} = \frac{N+2}{4N} \tag{1}$$

For a 4-to-1 Dickson converter, referring to Eq. (1), split-phase control is realized by imposing duty cycles of 0.375 on switches Q8 and Q5. This results in four equivalent circuits, as shown in Fig. 4, originally published in Ref. [18].

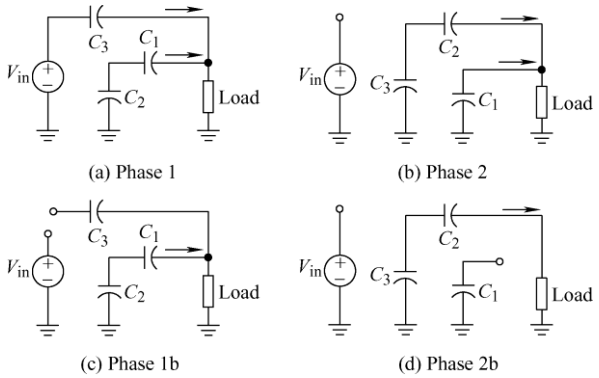

Fig. 4 Split-phase equivalent circuits of 4-to-1 Dickson converter

Fig. 4c and Fig. 4d show the two added circuit phases, Phase 1b and Phase 2b. In Phase 1b, the early switch-off of Q8 disconnects the input source and C_3 from the circuit, while in Phase 2b, the early switch-off of Q5 disconnects C_1 from the circuit. This way, the charging and discharging of capacitors C_3 and C_1 are controlled such that, assuming all flying capacitors are equal in capacitance value, the differences in voltage between the equivalent circuit branches for both Phase 1 and Phase 2 are eliminated.

For split-phase control to effectively reduce the equivalent circuit voltage differences, a small inductor is required to be added between the output node and the load [14-15, 18]. This ensures that the current continues to flow to the load throughout the switching

cycle, thereby ensuring smooth phase transitions.

As shown in the simulation results in Fig. 5, split-phase operation of the Dickson converter greatly reduces the equivalent circuit branch voltage differences during switching, and thus also greatly reduces the effect of charge redistribution in the Dickson converter.

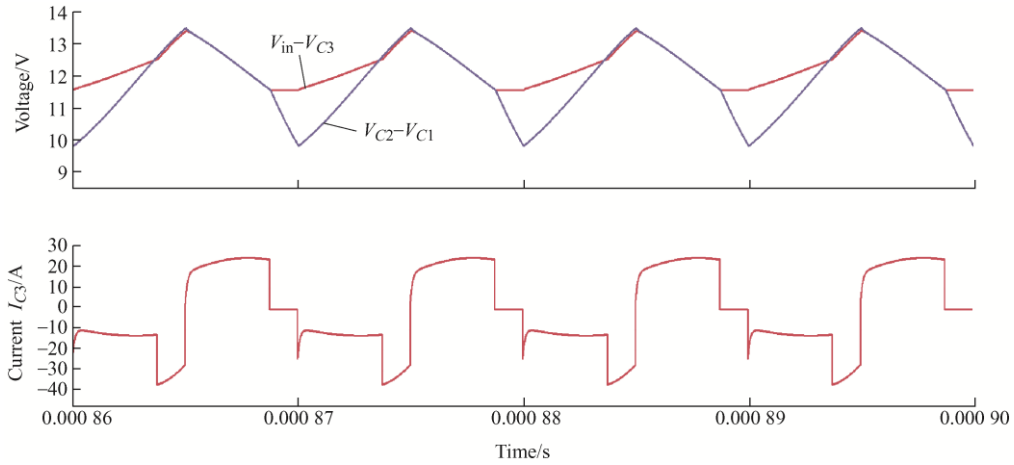

Fig. 5 Simulated Phase 1 branch voltage and flying capacitor C_3 behavior of split-phase 4-to-1 Dickson converter

3 Simulations and analysis of flying capacitor mismatch

The split-phase control theory presented in Ref. [18] was derived with the assumption that all flying capacitors in the Dickson SC circuit were of equal capacitance. As was discussed in the previous section, split-phase control eliminates the effects of charge redistribution by controlling the charging and discharging of the Dickson converter's flying capacitors. If the flying capacitors are mismatched, their unequal charge and discharge rates will cause voltage differences to appear between the equivalent circuit branches during switching. This in turn results in split-phase control not fully compensating for charge redistribution within the Dickson converter, potentially hampering the performance of the split-phase Dickson topology.

Simulations were performed on the 4-to-1 split-phase Dickson converter to investigate the sensitivity of the topology to mismatch in flying capacitor size. For each simulation, individual flying capacitors had their capacitance varied by either +20% or –20%, to reflect widely available manufacturing tolerances as well as the impact of the different DC blocking voltages, with the remaining flying capacitors held at a nominal value. The simulation parameters used are summarized in Tab. 1.

As a baseline scenario, Fig. 6 shows the Phase 1

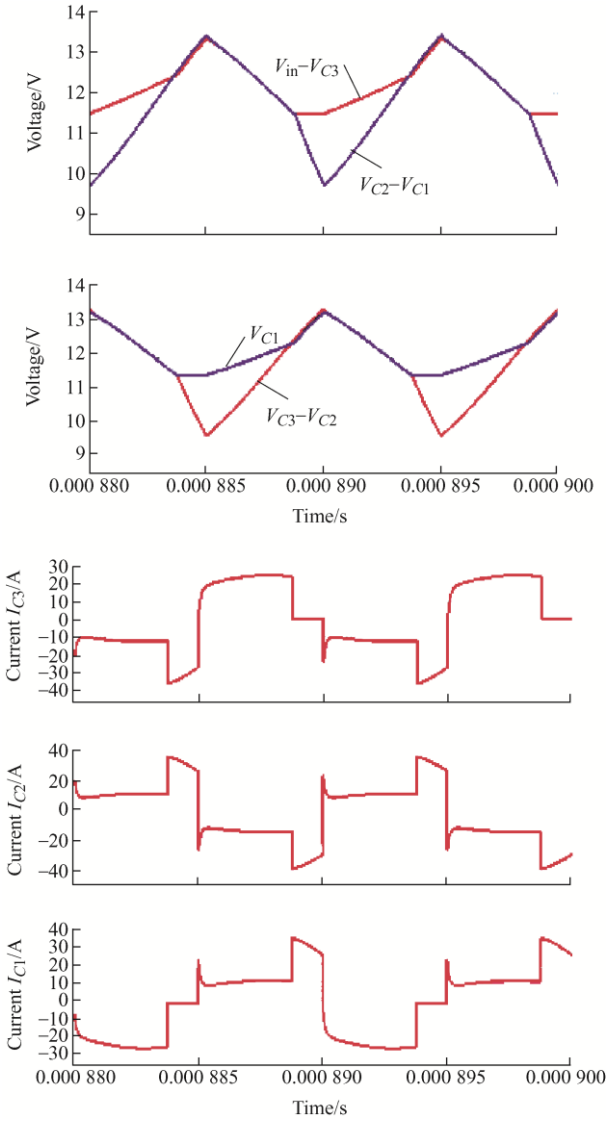

Fig. 6 Ideal (no mismatch) simulated equivalent circuit branch voltage waveforms and flying capacitor currents for 4-to-1 split-phase Dickson SCC

and Phase 2 equivalent circuit branch voltage waveforms and flying capacitor currents when all flying capacitors were matched at their nominal capacitances as listed in Tab. 1.

For comparison, Fig. 7 shows the Phase 1 and Phase 2 equivalent circuit branch voltage waveforms, as well as flying capacitor current waveforms, when a –20% variance is applied to flying capacitor C_3.

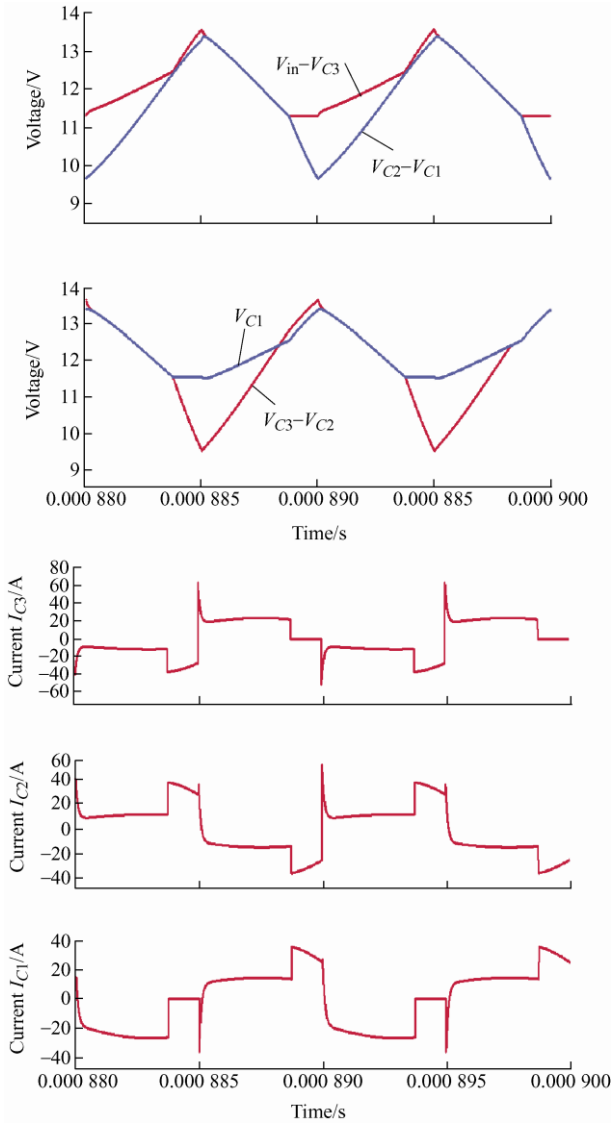

Fig. 7 Simulated equivalent circuit branch voltage waveforms and flying capacitor currents for 4-to-1 split-phase Dickson SCC, with variance of –20% on C_3

Compared to the baseline case, the simulation results for the scenario with mismatched flying capacitors show noticeable differences between the equivalent circuit branch voltages at the instance where switching takes place. Correspondingly, when switching does occur, spikes of around 60 A can be observed within the flying capacitors' current waveforms. Similar capacitor current spikes and differences in branch voltages during switching have been observed in simulations with variances in capacitance applied to other flying capacitors as well. Tab. 2 and Tab. 3 provides a quantitative summary of the results from the flying capacitor mismatch analysis, regarding the equivalent circuit branch voltage differences observed, as well as the maximum currents seen by each flying capacitor for each scenario. It is noted that when different R_{DS} and ESR values are used, the magnitudes of the current spikes will be different. Nevertheless, the current spikes will still be present due to flying capacitor mismatch.

Tab. 2 Summary of capacitor mismatch analysis simulations-Branch voltage differences

Scenario	C_3 size/μF	C_2 size/μF	C_1 size/μF	Branch voltage difference (Phase 1)	Branch voltage difference (Phase 2)
Ideal	47.00	47.00	47.00	–0.09	0.09
C_3–20%	37.60	47.00	47.00	0.28	0.27
C_3+20%	56.40	47.00	47.00	–0.32	–0.02
C_2–20%	47.00	37.60	47.00	–0.33	0.33
C_2+20%	47.00	56.40	47.00	0.06	–0.07
C_1–20%	47.00	47.00	37.60	–0.27	–0.27
C_1+20%	47.00	47.00	56.40	0.02	0.33

Tab. 3 Summary of capacitor mismatch analysis simulations-Maximum capacitor currents

Scenario	C_3 size/μF	C_2 size/μF	C_1 size/μF	$I_{C3\text{-max}}$ /A	$I_{C2\text{-max}}$/A	$I_{C1\text{-max}}$ /A
Ideal	47.00	47.00	47.00	36.89	36.89	36.87
C_3–20%	37.60	47.00	47.00	64.14	52.30	36.29
C_3+20%	56.40	47.00	47.00	35.99	62.31	62.31
C_2–20%	47.00	37.60	47.00	62.66	62.86	62.86
C_2+20%	47.00	56.40	47.00	36.71	36.71	36.69
C_1–20%	47.00	47.00	37.60	36.47	52.50	64.30
C_1+20%	47.00	47.00	56.40	62.02	62.02	35.97

As shown in Tab. 2 and Tab. 3, only the scenario in which a +20% variance was applied on capacitor C_2 did not result in significant capacitor current spikes. The waveforms obtained from simulation of this scenario can be seen in Fig. 8.

The output node-voltage equations for the Phase 1 and Phase 2 equivalent circuits are shown in Eqs. (2)-(3), respectively.

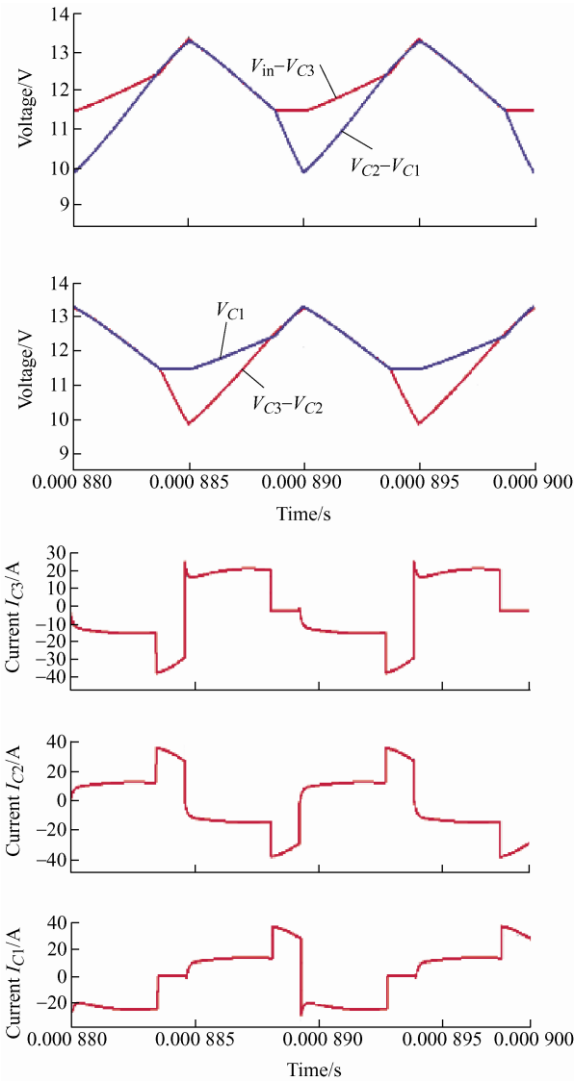

Fig. 8 Simulated equivalent circuit branch voltage waveforms and flying capacitor currents for 4-to-1 split-phase Dickson SCC, with variance of +20% on C_2

$$\Delta V_{n\_\text{Phase1}} = (V_{\text{in}} - V_{C3}) - (V_{C2} - V_{C1}) \tag{2}$$

$$\Delta V_{n\_\text{Phase2}} = (V_{C3} - V_{C2}) - V_{C1} \tag{3}$$

Referring to Eqs. (2)-(3), and the simulation results from the ideal scenario, it can be seen in Tab. 2, for the ideal scenario, the voltage difference between the branch voltages during the transition to Phase 1 was a negative value [$(V_{\text{in}}-V_{C3})<(V_{C2}-V_{C1})$], while the voltage difference during the transition to Phase 2 was a positive value [$(V_{C3}-V_{C2})>V_{C1}$]. When the size of capacitor C_2 was increased, its resultant decreased voltage ripple meant that the terms $(V_{C2}-V_{C1})$ and $(V_{C3}-V_{C2})$ became smaller compared to the ideal scenario. Consequently, the voltage differences during switching also became smaller in magnitude. This was the reason why a +20% variance on capacitor C_2 did not result in any significant current spikes through the flying capacitors.

The results shown in Tab. 2 and Tab. 3 show that in almost all cases, variance in flying capacitor values resulted in comparatively large differences between the equivalent circuit branch voltages during switching, and correspondingly, current spikes of around 60 A through the flying capacitors. This clearly indicates that the split-phase Dickson converter exhibits a significant sensitivity pertaining to variances in the sizes of the flying capacitors relative to each other; the unequal capacitor charging and discharging rates caused by capacitor mismatch results in split-phase control not fully eliminating the problem of charge redistribution.

In a scenario where all flying capacitors have a different capacitance, the current transients through the flying capacitors resulting from uneven charging and discharging of flying capacitors could be much higher. As an example, Fig. 9 shows the branch voltage and capacitor current waveforms obtained from a simulation of the 4-to-1 split-phase Dickson SCC with truly mismatched flying capacitors. In this simulation, capacitor C_3 had a size of 56.4 μF, capacitor C_2 had a value of 37.6 μF, and capacitor C_1 had a value of 47 μF. The maximum voltage difference observed was during the transition to Phase 1, with the magnitude of voltage difference being 0.543 V. This resulted in current spikes of up to 97 A through the flying capacitors during this transition, highlighting the split-phase Dickson converter's sensitivity to flying capacitor mismatch.

In practice, the current spikes resulting from charge redistribution due to mismatched flying capacitors contribute to additional switching and conduction losses. Furthermore, the current spikes and/or voltage noise resulting from charge redistribution could cause damage to circuit components. It follows that, as a conclusion to this analysis, for best performance, the flying capacitors of the split-phase Dickson converter should be matched in capacitance as closely as possible, to reduce the effects of charge redistribution arising from unequal capacitor charging/discharging caused by mismatch of capacitors. Unfortunately, due to component tolerances and the de-rating of capacitors due to DC voltage bias,

the flying capacitor values in the split-phase Dickson converter may be different under operation.

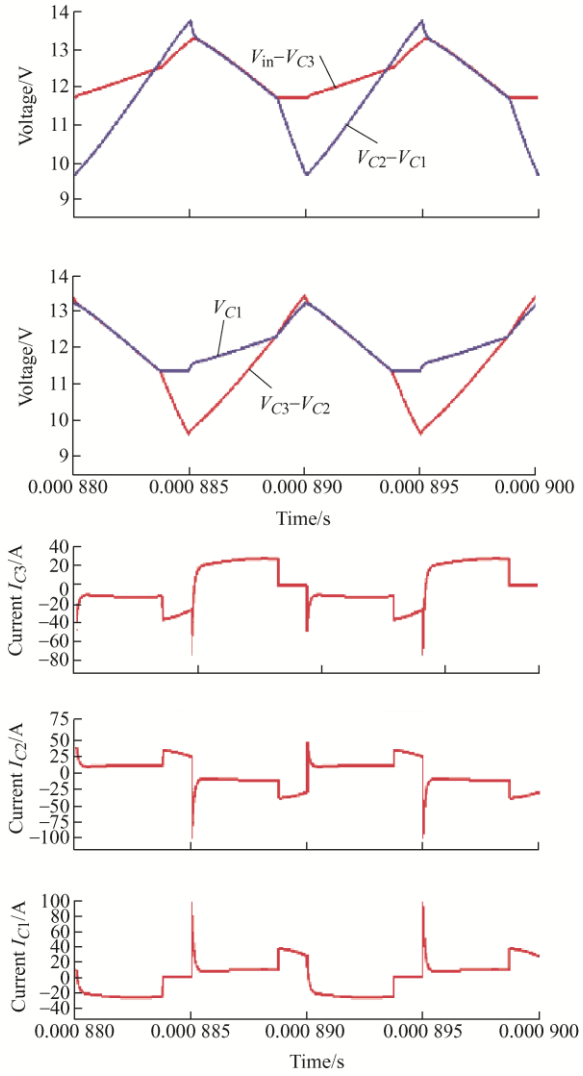

Fig. 9 Simulated equivalent circuit branch voltage waveforms and flying capacitor currents for 4-to-1 split-phase Dickson SCC (All flying capacitors mismatched)

4 Prototype design and considerations

The analysis from simulations regarding flying capacitor mismatch established that the split-phase Dickson converter works best when all flying capacitors are matched in capacitance as closely as possible. In practice, the flying capacitors for SCCs are typically constructed using ceramic capacitors because of their small package and low ESR values. However, ceramic capacitors have an inherent disadvantage in which their capacitances decrease when a DC voltage is applied across them. Therefore, the de-rating of the ceramic capacitors must be considered when designing the flying capacitors for the split-phase Dickson converter.

For the design of the 48 V to 12 V, 35 A split-phase Dickson converter prototype, the actual values of the three flying capacitors expected under operating conditions were matched to 60 μF, using de-rating curves provided by the component manufacturers. Tab. 4 shows the components used to construct the three flying capacitors, their expected de-rating at the required DC bias levels for each flying capacitor (based on the capacitors' datasheets), and the corresponding number of units required to construct each capacitor.

Tab. 4 Flying capacitor values and quantities used for prototype, based on de-rating

Capacitor size and nominal capacitance	Expected DC bias voltage/V	Expected de-rating at DC bias(%)	Per-unit capacitance at expected DC bias/μF	Units needed for 60 μF
1 210, 4.7 μF (Capacitor C_3)	36	–57	2.02	30
1 210, 10 μF (Capacitor C_2)	24	–42	5.8	10
1 206, 10 μF (Capacitor C_1)	12	–40	6	10

Along with ceramic capacitor de-rating, another source of mismatch between the flying capacitors is manufacturing tolerance. This is typically ±20% for ceramic capacitors. Unlike ceramic capacitor de-rating, the variance of capacitance due to manufacturing tolerance is much more difficult to predict. Due to this, as well as the part-to-part variance in the de-rating curves of the ceramic capacitors, an in-circuit estimation method was developed to estimate the actual flying capacitor sizes based on their voltage waveforms obtained during testing. This in-circuit estimation method would allow for verification of the capacitances of the flying capacitors in the prototype, as well as allow for later fine-tuning of the flying capacitors for better performance, if desired. The derivation of the in-circuit estimation method is described in detail in the following subsection. An example using one of the voltage waveforms obtained from prototype testing is also provided to demonstrate the method.

4.1 Derivation of in-circuit capacitance estimation method

As previously shown through simulation, the flying capacitors of the split-phase Dickson converter should be matched as closely as possible to minimize

the current spikes during switching transition. As this generally requires precise values of capacitance, it is desired that, in actual operation, the real capacitances of the flying capacitors be as close as possible to the expected capacitances at the level of expected DC voltage bias as specified by the capacitors' datasheets.

As previously explained in Section 2, the operation of the 4-to-1 split-phase Dickson converter consists of four circuit states. Two of these circuit states (Phases 1 and 2; Figs. 4a-4b [18]) have the same equivalent circuits as two-phase operation, while the other two states (Phases 1b and 2b; Figs. 4c-4d [18]) are sub-phases resulting from the application of split-phase control to the circuit [18]. Note that, while the equivalent circuits for Phases 1 and 2 consist of two branches that conduct current, the equivalent circuits for Phases 1b and 2b (the sub-phases) only consist of one circuit branch which conducts current. In both equivalent circuits, these branches are comprised of two flying capacitors and the load, connected in series, with the remaining flying capacitor disconnected from the circuit. Due to the small output inductor, the load current will remain approximately constant during this short sub-phase. Thus, the components comprising the sub-phase equivalent circuits carry the full load current for the duration of the sub-phases.

Referring to the equivalent circuits presented in Fig. 4 (Section 2), it can be seen that each flying capacitor carries the full load current for at least one sub-phase per switching cycle (capacitors C_2 and C_1 are connected in series with the load during Phase 1b, and capacitors C_3 and C_2 are connected in series with the load during Phase 2b). Therefore, since the load current is known, the above theory can be used to obtain the real value of the flying capacitors of the split-phase Dickson converter prototype using the flying capacitors' voltage waveforms using first principles. The time intervals where the flying capacitors carry the full load current can be identified by instances where the slope of the voltage waveforms are the steepest.

As an example, Fig. 10, obtained from prototype testing, shows the magnified waveform of capacitor C_3 at the instance where it is carrying the full output current (highlighted by the red line). The change in the voltage of this capacitor during this instance was measured to be 1.9 vertical oscilloscope divisions, over a time interval of 2.6 horizontal divisions. Given a scale of 250 mV per vertical division and 400 ns per horizontal division, the capacitor's voltage thus changed by 0.45 V over a time of 1.04 µs. Substituting these values, along with the output current of 35 A, into the capacitor's current-voltage relation equation (Eq. (4)), the real capacitance of C_3 as calculated using the waveform obtained from the prototype to be 78.7 µF.

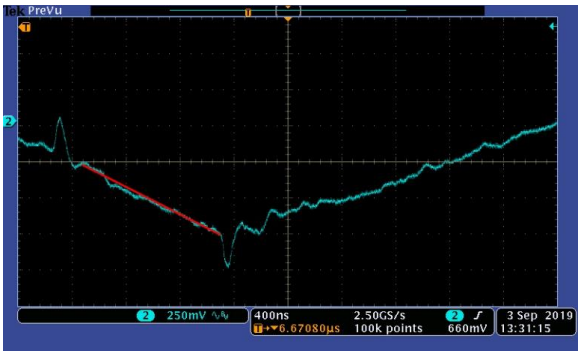

Fig. 10 Magnified voltage waveform of C_3(centered around the instance where it is carrying full load current)

$$C = I_{\text{Load}} \times \frac{\Delta t}{\Delta V} \tag{4}$$

4.2 Other circuit components

Regarding the circuit's switches, it is expected that switches Q6 and Q7 would need to block a maximum of $0.5\times V_{\text{in}}$, while all other switches are expected to block a maximum of $0.25\times V_{\text{in}}$. Tab. 5 shows other components used to construct the power stage of the 48-to-12 V split-phase Dickson converter.

Tab. 5 Other prototype components

Component	Manufacturer part	Number required
MOSFET (25 V rating)	SIRC16DP-T1-GE3	6
MOSFET (40 V rating)	BSC010N04LSI	2
Inductor (200 nH)	PA3790.201HL	1
Capacitor (2 200 µF)	63ZLH2200MEFC18X40	1

The use of the 2 200 µF electrolytic capacitor in the prototype was because of findings that input voltage ripple could interfere with the effective operation of the split-phase control method. To allow the input source to supply a constant (DC) current throughout operation, it is necessary to insert an input

filter (typically consisting of an input capacitor) between the input source and ground. The input capacitor charges and discharges throughout operation, thereby causing voltage ripple to appear at the input. Since the input source is in series with capacitor C_3 during Phase 1, any input voltage ripple will appear as a difference in branch voltages at the time of switching which is not compensated for by split-phase control. This input voltage ripple therefore causes branch voltage differences to appear whenever switching takes place. As shown in the simulation results in Fig. 11, steady-state operation with a 47 μF input capacitor resulted in voltage differences of up to 0.55 V during of up to 90 A during switching. These spikes were

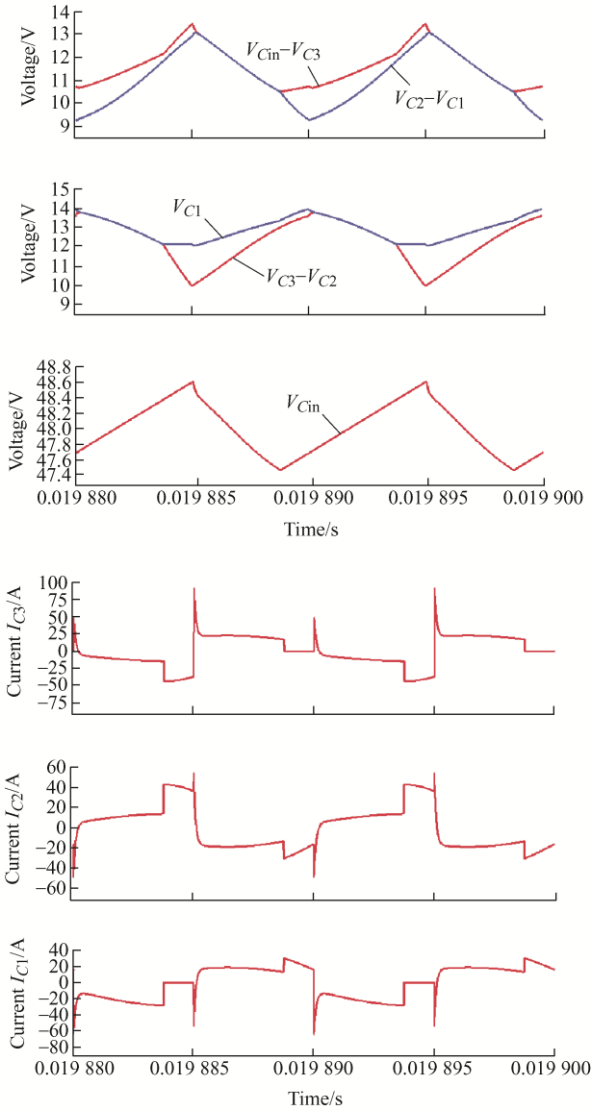

Fig. 11 Branch voltage, input voltage ripple, and flying capacitor current waveforms of simulated 48 V to 12 V, 35 A split-phase Dickson SCC with 47 μF flying capacitors, 47 μF input capacitor

switching, corresponding with capacitor current spikes nearly three times the output current of 35 A. In operation, the current spikes resulting from interference due to input voltage ripple will cause large switching and conduction losses, with the additional possibility of component damage due to the high amount of power the prototype is rated to handle.

When the simulations regarding input voltage ripple sensitivity was performed with different sizes of input capacitors, it was found that the effects of input voltage ripple on the operation of the split-phase Dickson converter could be suppressed through the use of a large input capacitor. As the main objective of prototype testing was to verify that the split-phase Dickson converter could be adapted for use in high-current applications, it was therefore decided that the risk of input voltage ripple interference in the prototype would be eliminated altogether through the use of the 2 200 μF electrolytic input capacitor.

The completed prototype measures approximately 2 in (1 in=2.54 cm)by 2 in, with the power stage taking up 1.125 in by 1.563 in. Figs. 12-13 show the top and bottom views of the power stage of the prototype. With a thickness of 0.5 in, the power stage takes up a volume of 0.88 in^3. The maximum output power is 420 W; this gives a power density of 477 W/in^3. It operates with a switching frequency of 100 kHz.

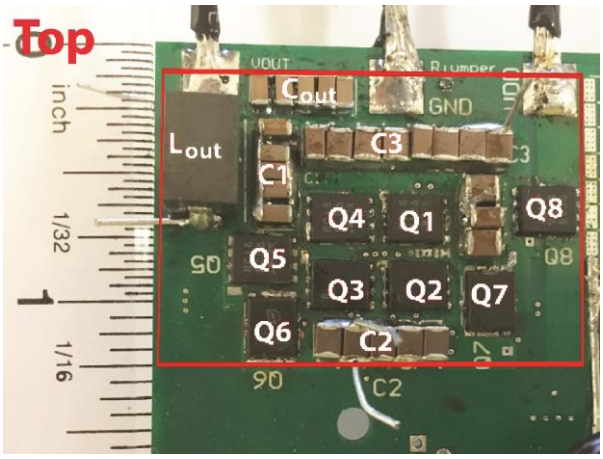

Fig. 12 Top view of power stage of 48 V to 12 V, 35 A split-phase Dickson SCC prototype (control components and input capacitor not shown)

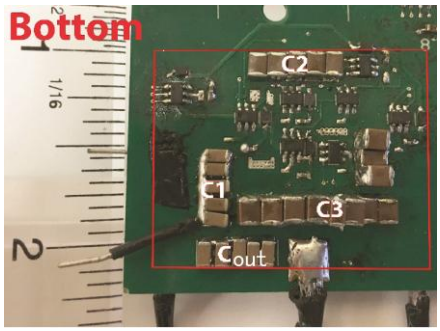

Fig. 13 Bottom view of power stage of 48 V to 12 V, 35 A split-phase Dickson SCC prototype

5 Test results

Fig. 14 shows the efficiency curve obtained from the prototype of the 48-to-12 V, 35 A split-phase Dickson SC converter, with the circuit components and configuration as outlined in Tabs. 4-5.

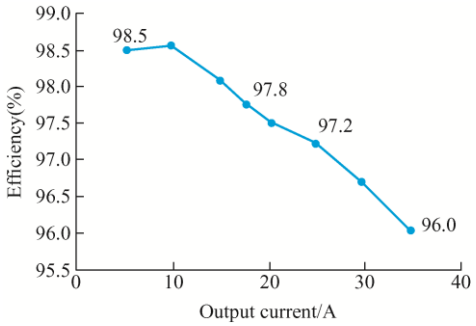

Fig. 14 Efficiency curve for 48 V to 12 V, 35 A split-phase Dickson converter(initial configuration)

The prototype, with the initial configuration as summarized in Tab. 4 and Tab. 5, achieved a peak efficiency of 98.6% at 1/4 load, and a full load efficiency of 96.0%. Utilizing a desk fan for cooling, the maximum temperature recorded on the prototype during full-load operation was 80 ℃. Fig. 15 shows the thermal image of the top side of the prototype during full-load operation.

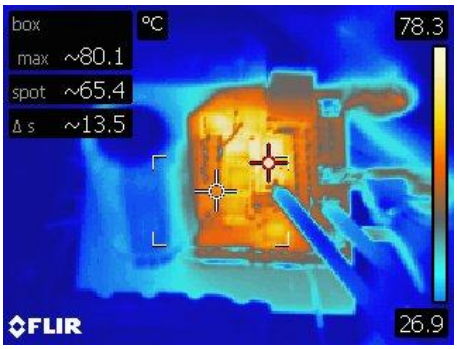

Fig. 15 Thermal image of top side of prototype at full load(initial configuration)

Fig. 16 shows the loss breakdown of the 48 V to 12 V split-phase Dickson converter at 35 A.

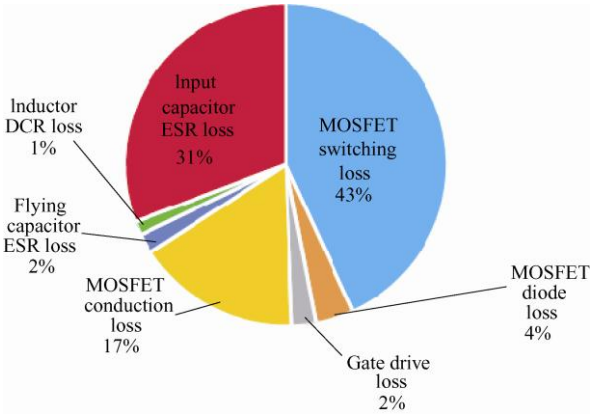

Fig. 16 Loss breakdown chart for Dickson converter prototype

The loss breakdown chart shows that the predominant cause of power loss at full load is MOSFET switching loss at 43%, followed by the loss due to the electrolytic input capacitor.

Figs. 17-19 show the voltage waveforms for the flying capacitors C_1, C_2, and C_3, respectively, at full load.

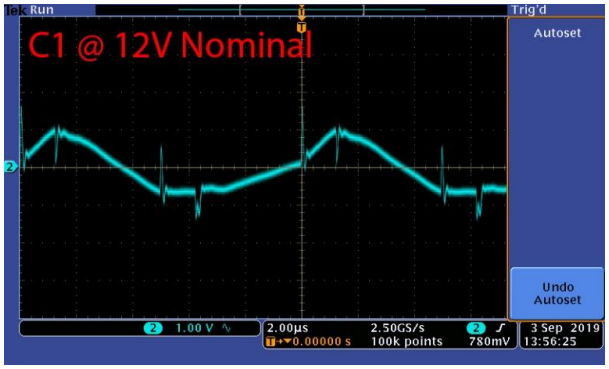

Fig. 17 Voltage waveform of flying capacitor C_1 at full load(using capacitors as designed in Tab. 4)

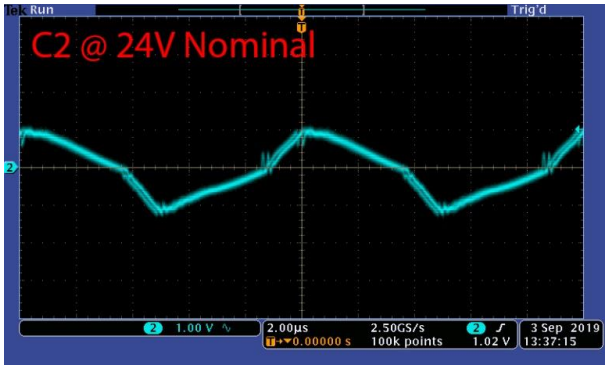

Fig. 18 Voltage waveform of flying capacitor C_2 at full load(using capacitors as designed in Tab. 4)

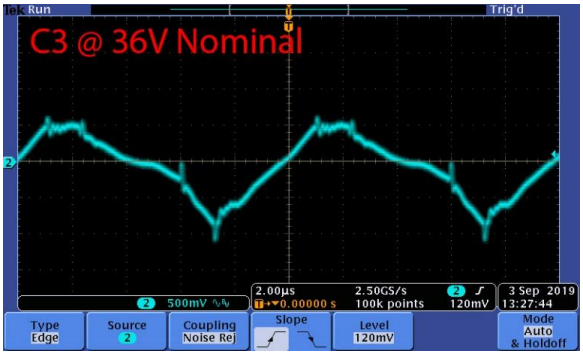

Fig. 19 Voltage waveform of flying capacitor C_3 at full load(using capacitors as designed in Tab. 4)

To investigate whether mismatch was indeed present among the flying capacitors, as well as whether there were any discrepancies between the expected derating values and the actual derating values of the flying capacitors, measurements were performed using the flying capacitors' voltage waveforms to determine the real value of the prototype's flying capacitors. This was accomplished using the in-circuit estimation method outlined in Section 4.1. Two groups of measurements were made; the flying capacitors were measured under both full-load (35 A output current) operation, as well as half-load (15 A output current) operation. The flying capacitor size measurements obtained from the full-load and half-load measurements were very close in value to each other. Tab. 6 shows the flying capacitor sizes as measured under full-load operation, and Tab. 7 shows the flying capacitor sizes as measured under half-load (15 A) operation.

Tab. 6 Expected vs. calculated flying capacitor sizes of prototype (35 A measurements)

Flying capacitor and total nominal capacitance/µF	Expected voltage de-rating (%)	Expected total capacitance /µF	Real capacitance (Full load measurements) /µF	Actual de-rating (%)
C_3=30×4.7	–57	60.6	78.7	–44.2
C_2=10×10	–42	58.0	39.2	–60.8
C_1=10×10	–40	60.0	54.0	–46.0

Tab. 7 Expected vs. calculated flying capacitor sizes of prototype (15 A measurements)

Flying capacitor and total nominal capacitance/µF	Expected voltage de-rating (%)	Expected total capacitance /µF	Real capacitance (Half load measurements) /µF	Actual de-rating (%)
C_3=30×4.7	–57	60.6	78.0	–44.7
C_2=10×10	–42	58.0	40.0	–60.0
C_1=10×10	–40	60.0	55.4	–44.6

A comparison between the actual and expected flying capacitor values in Tabs. 6-7 show that, while some flying capacitors experienced less de-rating than expected, others experienced more de-rating than expected. The most significant anomalies between the measured and expected capacitance values were observed in capacitors C_3 and C_2. The ceramic capacitors used for C_3 were seen to have de-rated by around 44% at 36 V during testing, less than the 57% de-rating specified from its datasheet. The capacitors used for C_2 were seen to have de-rated by around 60% at 24 V during testing, significantly more than the 42% de-rating specified from its datasheet. The capacitors used for C_1 de-rated roughly as expected, but its measured capacitance is still a bit different from the expected capacitance. These measurement results exemplify the variances in capacitance that can result from measurement errors in both the de-rating curves and experimental values, as well as manufacturing tolerance and effects of the actual in-circuit conditions when the capacitors are used in a switching converter.

The analysis of the actual flying capacitor values concludes that potential inaccuracies in the supplied ceramic capacitor de-rating curves, together with manufacturing tolerances, are primary sources of flying capacitor mismatch in practical implementations of the Dickson converter. Therefore, some fine tuning may be necessary to improve the performance of the split-phase Dickson converter. However, it should be noted that while some of the capacitor de-rating curves used during initial design may have been found to be inaccurate, the prototype, with its flying capacitors matched solely through referral to the de-rating curves still delivered satisfactory performance.

To determine whether matched flying capacitors would result in any improvement of performance, additional ceramic capacitors were added to both C_2 and C_1 to bring their capacitances closer to the value of C_3. 9 more capacitors were added to capacitor C_2 (for a total of 19 capacitors for C_2), while 5 more capacitors were added to capacitor C_1 (for a total of 15 capacitors for C_1). A comparison of efficiency curves between operating the prototype with fully matched flying capacitors and operating the prototype with the flying capacitors as initially designed in Tab. 4, is

shown in Fig. 20.

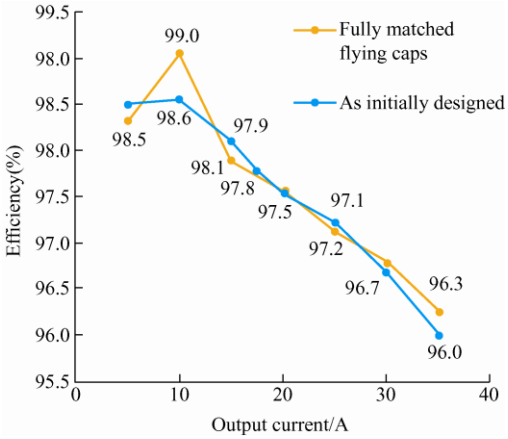

Fig. 20 Comparison of efficiency curves for 48 V to 12 V split-phase Dickson converter with fully matched flying capacitors and the prototype with flying capacitors as initially designed in Tab. 4

The prototype with its flying capacitors matched saw an overall improvement in efficiency by 0.3%-0.4%, with a peak efficiency of 99% at 1/4 load (versus 98.6%), and a full load efficiency of 96.3% (versus 96.0%). The loss reduction between the prototype operating with fully matched flying capacitors and the prototype operation with components as initially designed was around 1 W. The power loss at a full load efficiency of 96% (attained by the prototype during initial testing, operating as initially configured) was 16 W; therefore, the percentage of loss reduction between operation with fully-matched flying capacitors and operation with flying capacitors as initially designed was 6.25%.

The temperature profile of the prototype has also seen slight improvements, with a maximum temperature of 78.7 ℃ recorded a full-load operation. Fig. 21 shows the thermal image of the top side of the prototype with fully matched flying capacitors during full-load operation.

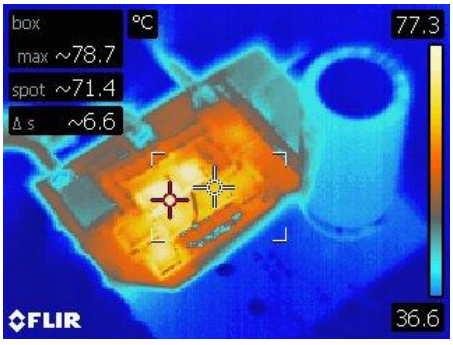

Fig. 21 Thermal image of top side of prototype at full load(fully matched flying capacitors)

Therefore, it can be concluded from prototype testing that it is important to ensure that the sizes of flying capacitors of the split-phase Dickson converter are matched as closely as possible, giving consideration that ceramic capacitors de-rate when subjected to a DC voltage bias. This ensures optimal performance of the split-phase Dickson converter. However, it has also been shown that designing the flying capacitors based on the supplied capacitor de-rating curves, even with the capacitors de-rating far more than the suppliers' de-rating curves showed, still resulted in reliably performing prototype.

6 Conclusions

The work presented throughout this paper has shown that the split-phase Dickson converter could be successfully adapted for high-current applications of up to 35 A. In doing so, an important consideration was identified, concerning the possibility of mismatched flying capacitors. Since split-phase control achieves capacitor voltage matching during switching by controlling the flying capacitors' charging and discharging, mis-matched flying capacitors, with unequal charging and discharging rates, will result in split-phase control not fully achieving this voltage matching during switching. In practice, the primary causes of mismatched flying capacitors are ceramic capacitor de-rating and manufacturing tolerance. The flying capacitors should be designed using supplied de-rating curves to minimize the possibility of mismatch. However, considering the possibility of inaccuracies in the de-rating curves, as well as manufacturing tolerances, the flying capacitor configurations may need to be verified and/or fine-tuned using in-circuit testing techniques to allow for performance improvements for the split-phase Dickson converter. This problem should be solved for large volume production of the split-phase Dickson switched-capacitor converter.

As shown in the loss breakdown chart (Fig. 10), a major source of power loss is the input capacitor. Currently, a large electrolytic capacitor is used for the input capacitor, since other simulations performed on the split-phase Dickson converter has shown that the topology experiences sensitivity to voltage ripple

caused by the presence of an input capacitor. Work is currently underway to develop a method for mitigating this input voltage ripple. This would in turn allow for the input capacitor to be implemented with smaller (ceramic) capacitors, thus potentially improving the efficiency of the split-phase Dickson converter. Furthermore, considering the high switching losses in the split phase prototype, future work may also investigate the possibility of using wide-band-gap devices to reduce the switching losses of the split-phase Dickson converter.

References

[1] X Li, S Jiang. Google 48 V power architecture. *2017 IEEE Applied Power Electronics Conference and Exposition (APEC)*, Tampa, FL, 2017, Keynotes presentation.

[2] T S Liu. Novel high power density topologies and control for the point-of-load(POL) application. Kingston: Queen's University, 2016.

[3] D C Reusch. High frequency, high power density integrated point of load and bus converters. Blackburg: Virginia Polytechnic Institute and State University, 2012.

[4] V W Ng, M D Seeman, S R Sanders. Minimum PCB footprint point-of-load DC-DC converter realized with switched-capacitor architecture. *2009 IEEE Energy Conversion Congress and Exposition*, San Jose, CA, 2009: 1575-1581.

[5] Y Cao, Z Ye. Simulation and analysis of switched capacitor DC-DC converters for use in battery electric vehicles. *2015 IEEE Power and Energy Conference at Illinois (PECI)*, Champaign, IL, 2015: 1-6.

[6] M S Makowski, D Maksimovic. Performance limits of switched-capacitor DC-DC converters. *Proceedings of PESC' 95-Power Electronics Specialist Conference*, Atlanta, GA, USA, 1995: 1215-1221.

[7] S R Sanders, E Alon, H P Le, et al. The road to fully integrated DC-DC conversion via the switched-capacitor approach. *IEEE Transactions on Power Electronics*, 2013, 28(9): 4146-4155.

[8] M D Seeman, S R Sanders. Analysis and optimization of switched-capacitor DC-DC converters. *IEEE Transactions on Power Electronics*, 2008, 23(2): 841-851.

[9] M D Seeman. A design methodology for switched-capacitor DC-DC converters. Berkeley: University of California, 2009.

[10] V W Ng, S R Sanders. Switched capacitor DC-DC converter: Superior where the buck converter has dominated. Berkeley: University of California, 2011.

[11] Y Lei, R C N Pilawa-Podgurski. Analysis of switched-capacitor DC-DC converters in soft-charging operation. *2013 IEEE 14th Workshop on Control and Modeling for Power Electronics (COMPEL)*, Salt Lake City, UT, 2013: 1-7.

[12] Y Lei, R C N Pilawa-Podgurski. Soft-charging operation of switched-capacitor DC-DC converters with an inductive load. *2014 IEEE Applied Power Electronics Conference and Exposition-APEC 2014*, Fort Worth, TX, 2014: 2112-2119.

[13] S Jiang, S Saggini, C Nan, et al. Switched tank converters. *IEEE Transactions on Power Electronics*, 2019, 34(6): 5048-5062.

[14] Y Lei, Z Ye, R C N Pilawa-Podgurski. A GaN-based 97% efficient hybrid switched-capacitor converter with lossless regulation capability. *2015 IEEE Energy Conversion Congress and Exposition (ECCE)*, Montreal, QC, 2015: 4264-4270.

[15] B B Macy, Y Lei, R C N Pilawa-Podgurski. A 1.2 MHz, 25 V to 100 V GaN-based resonant Dickson switched-capacitor converter with 1 011 W/in^3 (61.7 kW/L) power density. *2015 IEEE Applied Power Electronics Conference and Exposition (APEC)*, Charlotte, NC, 2015: 1472-1478.

[16] C K Tse, S C Wong, M H L Chow. On lossless switched-capacitor power converters. *IEEE Transactions on Power Electronics*, 1995, 10(3): 286-291.

[17] Q Li, J Chen, D Jiang. Periodic variation in the effect of switching frequency on the harmonics of power electronic converters. *Chinese Journal of Electrical Engineering*, 2020, 6(3): 35-45.

[18] Y Lei, R May, R Pilawa-Podgurski. Split-phase control: Achieving complete soft-charging operation of a Dickson switched-capacitor converter. *IEEE Transactions on Power Electronics*, 2016, 31(1): 770-782.

[19] D Gunasekaran, F Z Peng. Design of GaN based ultra-high efficiency, high power density resonant Dickson converter for high voltage step-down ratio. *2019 IEEE Energy Conversion Congress and Exposition (ECCE)*, Baltimore, MD, USA, 2019: 845-852.

[20] O Jong, Q Li, F C Lee, et al. Loss model and optimization method for switched-capacitor divider for POL application. *2018 IEEE Energy Conversion Congress and Exposition (ECCE)*, Portland, OR, 2018: 3844-3850.

Richard(Yue) Sun received his BASc. degree in electrical engineering from Queen's University in Kingston, Ontario, Canada in 2019. He is currently working towards his MASc. degree at the Queen's Power Research Group at Queen's University in Kingston, Ontario, Canada. His current research conprises of the design and optimization of switched-capacitor converters for high current applications.

Samuel Webb is a PhD student at Queen's University. He received his Bachelor's degree from the Department of Electrical and computer Engineering at Queen's University in 2016, and began his graduate studies under Queen's accelerated 4+1 program.

Sam's current research interests are primarily focused on extremely high efficiency DC-DC converter topologies, switched-capacitor topologies, and control techniques for these converters.

Sam has authored several papers presented at both the ECCE and APEC conferences, receiving an Outstanding Presentation award at APEC 2018. He has also served as the Chapter Chair for the IEEE-PELS Kingston chapter since 2019. Sam has been awarded scholarships under both the Ontario Graduate Scholarship Program, and the NSERC Postgraduate Scholarships-Doctoral Program.

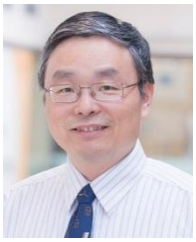

Yan-Fei Liu (Fellow of IEEE, 2013, Fellow of CAE, 2018) received his Bachelor and Master degrees from the Department of Electrical Engineering from Zhejiang University, China, in 1984 and 1987 and PhD degree from the Department of Electrical and Computer Engineering, Queen's University, Kingston, ON, Canada, in 1994.

He was a technical advisor with the Advanced Power System Division, Nortel Networks, in Ottawa, Canada from 1994 to 1999. Since 1999, he has been with Queen's University, where he is currently a professor with the Department of Electrical and Computer Engineering. His current research interests include digital control technologies for high efficiency, fast dynamic response DC-DC switching converter and AC-DC converter with power factor correction, resonant converters and server power supplies, and LED drivers. He has authored around 250 technical papers in the IEEE Transactions and conferences, and hold 35 U.S. patents. He has written a book on "High Frequency MOSFET Gate Drivers: Technologies and Applications", published by IET. He is also a principal contributor for two IEEE standards. He received "Modeling and Control Achievement Award" from IEEE Power Electronics Society in 2017. He received Premier's Research Excellence Award in 2000 in Ontario, Canada. He also received the Award of Excellence in Technology in Nortel in 1997.

Dr. Liu is the vice president of Technical Operations of IEEE Power Electronics Society (PELS, from 2017 to 2018). Dr. Liu serves as an editor of IEEE Journal of Emerging and Selected Topics of Power Electronics (IEEE JESTPE) since 2013. He is the general chair of ECCE 2019 held in Baltimore, USA in 2019. His major service to IEEE is listed below: a Guest Editor-in-Chief for the special issue of Power Supply on Chip of IEEE Transactions on Power Electronics from 2011 to 2013; a guest editor for special issues of JESTPE: Miniaturization of Power Electronics Systems in 2014 and Green Power Supplies in 2016; as co-general chair of ECCE 2015 held in Montreal, Canada, in September 2015; the chair of PELS Technical Committee (TC1) on Control and Modeling Core Technologies from 2013 to 2016; chair of PELS Technical Committee (TC2) on Power Conversion Systems and Components from 2009 to 2012.